Relativistic splitting of surface states at Si-terminated surfaces of the layered intermetallic compounds RT_2Si_2 (R=rare earth; T=Ir, Rh)

I. A. Nechaev[1] and E. E. Krasovskii[2,3,4]

[1]*Centro de Física de Materiales CFM – MPC, Centro Mixto CSIC-UPV/EHU, 20018 Donostia/San Sebastián, Basque Country, Spain*

[2]*Departamento de Física de Materiales, Facultad de Ciencias Quíimicas, Universidad del Pais Vasco/Euskal Herriko Unibertsitatea, Apdo. 1072, 20080 Donostia/San Sebastián, Basque Country, Spain*

[3]*Donostia International Physics Center (DIPC), Paseo Manuel de Lardizabal 4, 20018 Donostia/San Sebastián, Basque Country, Spain*

[4]*IKERBASQUE, Basque Foundation for Science, 48013 Bilbao, Basque Country, Spain*

(Received 2 October 2018; published 17 December 2018)

We present an effective model for surface states at the Si-terminated (001) surface of ternary rare earth (R) intermetallic compounds RT_2Si_2 with the transition metal element T = Ir or Rh. The model is based on a fully *ab initio* derivation of the relativistic $\mathbf{k}\cdot\mathbf{p}$ Hamiltonian and is thereby capable of accurately reproducing the spin polarization of the spin-orbit split surface states, which is very different from the classical Rashba effect. The reliable treatment of spin in our model enables a predictive analysis of the effect of magnetic exchange interaction of the surface-state electrons with ferromagnetically ordered $4f$ moments of the subsurface rare-earth layer in the magnetic phases of the RT_2Si_2 compounds.

DOI: 10.1103/PhysRevB.98.245415

I. INTRODUCTION

In the last two decades, the effort in spin-based information technology has motivated the search for new materials as well as for spintronics-related phenomena at surfaces and interfaces, in which the spin-orbit interaction (SOI) plays the key role [1–3]. In this regard, the few-layer structures or crystal surfaces hosting two-dimensional (2D) Rashba or Dirac surface states are very promising for controlling spin transport, spin accumulation, and spin polarized tunneling [4–9].

Recently, the RT_2Si_2 intermetallic compounds have been suggested to be a promising candidate for applications in spin-based devices [10–14]. Here R stands for a rare-earth element (Sm, Eu, Gd, Ho, or Yb) and T for a transition metal (TM) element (Ir or Rh). These compounds have a layered $ThCr_2Si_2$ type structure [15], with the rare-earth layers separated by Si-T-Si trilayers. In the magnetic phase, the rare-earth $4f$ magnetic moments are ferromagnetically ordered within the layer and antiferromagnetically aligned with the nearest-neighbor rare-earth layers [11,12,16,17]. The Si-T-Si-R four layer of the Si-terminated (001) surfaces of these ternary compounds gives rise to fascinating surface phenomena brought about by the competition between the Rashba effect and magnetic exchange interaction, where the former causes a momentum-dependent spin-orbit splitting of surface states and the latter introduces a Zeeman-like splitting of states with the opposite spin.

To facilitate the treatment of the 2D electronic system as part of a nanodevice and perform large-scale quantum transport calculations, one must separate out its essential properties from those of the actual three-dimensional (3D) system. This is traditionally achieved by constructing an effective $\mathbf{k}\cdot\mathbf{p}$ Hamiltonian capable of a simple and accurate model description of the 2D states. A famous and classical example of such a Hamiltonian is the Rashba model [18,19]. However, it relies on the spin of the state as a dynamic variable, so it cannot be applied to systems with strong spin-orbit interaction in which an electron state cannot be ascribed a definite spin. Here we report an effective model to study the competing effect of the two fundamentally different spin-splitting mechanisms on the behavior of surface states. Our model is based on the recently suggested method [20] to *microscopically* derive the $\mathbf{k}\cdot\mathbf{p}$ Hamiltonian from relativistic wave functions. Strictly speaking, it is $\mathbf{k}\cdot\boldsymbol{\pi}$, where $\boldsymbol{\pi}$ includes the SOI term in a nonperturbative manner in contrast to many approaches that employ a nonrelativistic (or scalar-relativistic) basis. We have extended this method to ensure a transfer of the momentum-dependent spin polarization of a subset of the true *ab initio* states to the states of the reduced Hilbert space of the effective model. This model offers a tool to study the modification of the spin-orbit split states by continuously varying a model parameter accounting for magnetic exchange interaction.

In this paper we apply the model to the Si-terminated surfaces of the RT_2Si_2 compounds with T= Ir or Rh. We start from *ab initio* band-structure calculations for the surfaces of two representatives—the paramagnetic $YbIr_2Si_2$ and $YbRh_2Si_2$, which underlie the derivation of $\mathbf{k}\cdot\mathbf{p}$ Hamiltonians for our effective model. In our *ab initio* calculations we have found that the TM-related surface states exhibit a $\mathbf{k}$-dependent splitting and spin polarization very different from the classical Rashba effect. On a microscopic level, this manifests itself in a curious hidden spin polarization of the surface states: for a given $\mathbf{k}$ the spin at the two TM sublattices has the opposite sign. Because our model has absorbed all the microscopic information it closely reproduces the nontrivial behavior of both the surface state dispersion and their observable spin structure. Furthermore, the knowledge of the *true* spin structure (as opposed to pseudospin or effective spin) at the $\mathbf{k}\cdot\mathbf{p}$ model

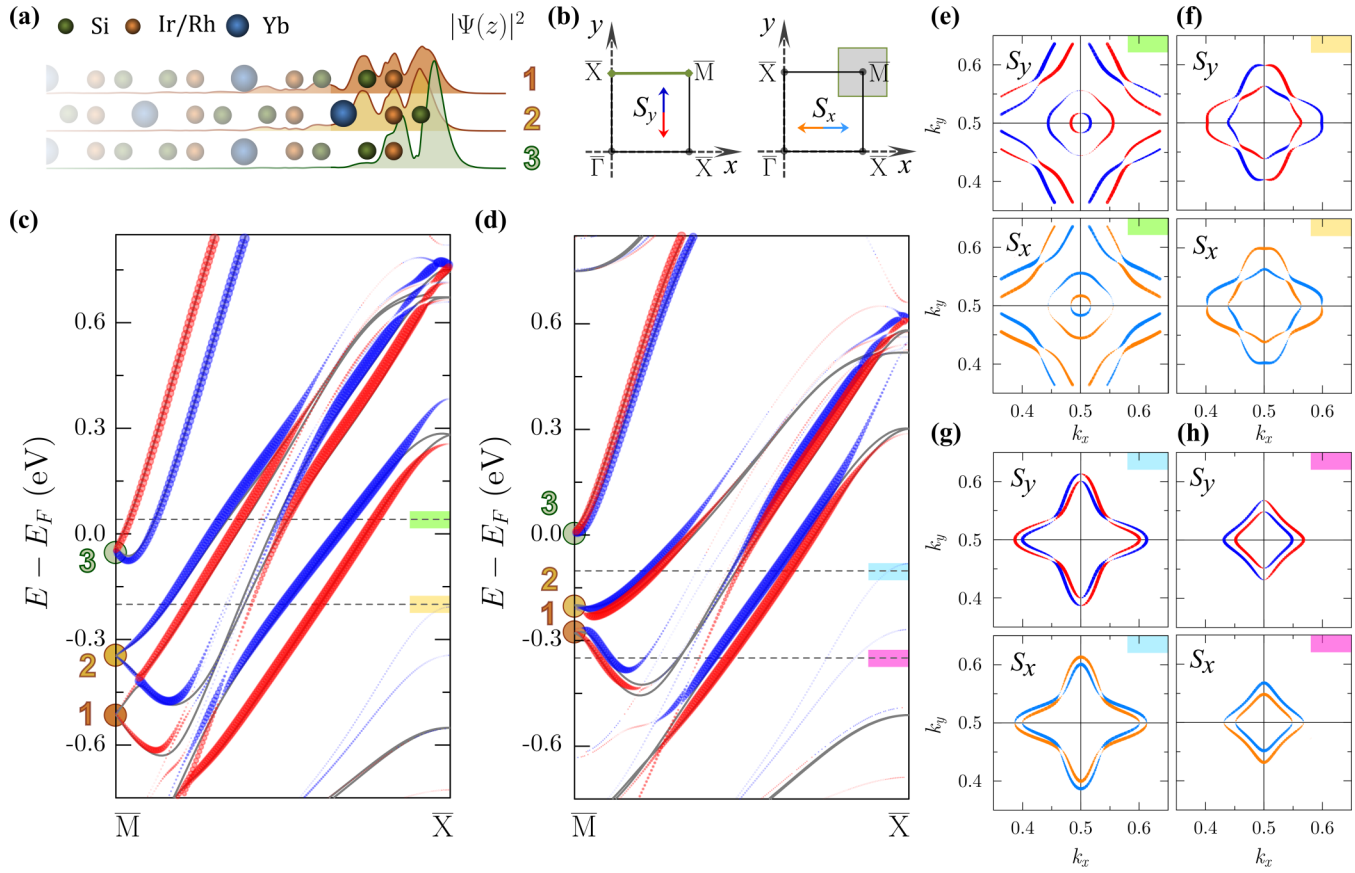

FIG. 1. (a) Upper half of the unit cell of the bulk-truncated symmetric 31-layer slab with the equivalent Si-terminated opposite surfaces and density profiles of the surface states at the $\bar{M}$ point. (b) Upper right quadrant of the surface Brillouin zone showing the $\bar{M}$-$\bar{X}$ line, the CEC region of $\mathbf{k}$ space around $\bar{M}$, and the color code for the spin y and x projections. Band structure along $\bar{M}$-$\bar{X}$ for $YbIr_2Si_2$ (c) and $YbRh_2Si_2$ (d) by the *ab initio* Hamiltonian $H_{\mathbf{k}}^{\mathrm{LDA}}$ is shown by red ($S_y < 0$) and blue ($S_y > 0$) fat bands revealing the spin polarization calculated as in-plane spin projection onto the four outermost layers of the upper half of the slab. Gray lines are the band structure of the same surface in a 19-layer slab geometry (space group $P4/nmm$, No. 129), which simulates the behavior of the surface state bands near the $\bar{M}$ and $\bar{X}$ points in the semi-infinite limit (see also Ref. [14]). Spin-resolved *ab initio* CECs for the surface states of $YbIr_2Si_2$, (e) and (f), and $YbRh_2Si_2$, (g) and (h), are calculated at 0.05, −0.2, −0.1, and −0.35 eV, respectively.

level allowed us to simulate magnetic exchange interaction by a trivial Zeeman term. We then consider the surface states of our model as a prototype of those of a paramagnetic phase of an RT_2Si_2 compound and tune the relative strength of the competing spin-orbit and exchange interactions in order to illustrate how the surface states at the Si-terminated surface are influenced by the ferromagnetically ordered $4f$ moments of the subsurface rare-earth layer in a magnetic phase of this compound. The modification of the surface electronic structure suggested by the model is in full accord with the experimental ARPES (angle-resolved photoemission spectroscopy) observations and the corresponding *ab initio* calculations for magnetic phases of the RT_2Si_2 compounds [11,12,21].

II. METHOD AND RESULTS

We consider the Si-terminated (001) surface of two paramagnetic crystals $YbIr_2Si_2$ and $YbRh_2Si_2$ [22], which exemplify the surface electronic structure of a wide class of RT_2Si_2 compounds with Ir or Rh as the transition-metal element. We focus on the properties of the surface states at the Si-terminated (001) surface, Fig. 1(a), which we simulate by Si-terminated centrosymmetric 31-layer slabs of space group $P4/mmm$ (No. 123). The experimental crystal lattice parameters of $YbIr_2Si_2$ and $YbRh_2Si_2$ are taken from Ref. [23]. Band structure calculations with $4f$ electrons treated as part of the frozen core are performed with the extended linear augmented plane wave method [24] within the local density approximation (LDA) for the exchange-correlation functional using the full potential scheme of Ref. [25].

Figures 1(c) and 1(d) show the calculated spin-resolved band structure of the surface states of both compounds around the $\mathbf{k}$ point $\bar{M}$, which has the same symmetry as $\bar{\Gamma}$. At first glance, in the direction $\bar{M} \to \bar{X}$, the surface states demonstrate spin polarization typical of the Rashba effect: the spin expectation values of the two branches of the spin-orbit split state have opposite signs, and the spin is locked perpendicular to the momentum. In Fig. 1(a) the three surface states are numbered in order of increasing energy. The highest state $n = 3$ is largely localized near the outermost Si layer [marked by the green circles in Figs. 1(c) and 1(d)], whereas the lower surface states $n = 1$ and 2 (brown and orange circles) have the dominant contribution from the subsurface transition-metal atoms. State 3 will also be referred to as the Si surface state,

and states 1 and 2 as TM surface states. The spin-resolved picture suggests that while for $n = 3$ the Rashba parameter α_R is positive, for $n = 1$ and 2 it is negative. In the vicinity of $\bar{M}$, however, the behavior of the TM states strikingly deviates from the textbook Rashba splitting (especially for $YbIr_2Si_2$): both for $n = 1$ and for $n = 2$, the state is spin-orbit split, but the two branches have the same sign of the spin expectation value S_y (rather small for both branches), so they cannot be understood as *spin* split.

A detailed analysis of the Si surface state confirms the typical Rashba splitting and the characteristic spin-momentum locking around the point $\bar{M}$ within the gray region indicated in Fig. 1(b), see the two closed constant energy contours (CECs) in the center of Fig. 1(e). A similar situation is observed for the surface state 1 for momenta immediately outside the exotic region around $\bar{M}$, Fig. 1(h). The other TM-related surface state $n = 2$, both close to $\bar{M}$ and far from $\bar{M}$, has a complex spin structure of the CECs very different from the classical Rashba effect, see Figs. 1(e) and 1(f) for Ir and 1(g) for Rh.

We focus on this surface state because in all compounds of this family it crosses the Fermi level, so it is essential for transport properties. Clearly the traditional Rashba Hamiltonian is not sufficient here, so we will construct an effective $\mathbf{k}\cdot\mathbf{p}$ model following the *microscopic* approach of Ref. [20]. This method allows us to derive a $\mathbf{k}\cdot\mathbf{p}$ Hamiltonian of a desired size from *ab initio* wave functions as a second-order $\mathbf{k}\cdot\mathbf{p}$ expansion around a TRIM (time reversal invariant momentum) for systems with inversion symmetry. The size of the Hamiltonian is determined by the dimension of the Hilbert space spanned by physically chosen basis functions—*ab initio* spinor wave functions, which are unitary transformed to diagonalize the expectation value of the z component of the total angular momentum $\mathbf{J} = \mathbf{L} + \mathbf{S}$, see Ref. [20]. Here we will further develop the method to make it applicable to a surface simulated by a thick centrosymmetric slab and to ensure a transfer of the momentum-dependent spin polarization of the chosen *ab initio* states to the states of the reduced Hilbert space of the effective model.

In our study the basis comprises the surface states considered above: $n = 1$, 2, and 3. Being eigenfunctions of a centrosymmetric Hamiltonian $H_{\mathbf{k}}^{\mathrm{LDA}}$ at $\bar{M}$, they form six Kramers-degenerate pairs with spinor wave functions $\Psi_{m\mu}$ ($\mu =\uparrow$ or $\downarrow$ indicates the z projection of $\mathbf{J}$) grouped in three twin pairs with $m = 2n - 1$ and $m = 2n$. Since the $\bar{M}$ point is a TRIM, the spinors $\Psi_{m\mu}$ are also parity eigenfunctions. Thus, the symmetry properties of the basis functions are completely defined by the $\bar{M}$-point-projected Hamiltonian $H_{\mathbf{k}=\bar{M}}^{\mathrm{LDA}}$ of our 31-layer slab. It is noteworthy that in the spinor wave functions with $n = 3$ (the Si surface state) the largest weight is provided by the Si-atomic sphere, where p_z orbitals dominate, while for $n = 1$ and 2 (the TM surface states) the subsurface TM atomic spheres are most important, with the largest contribution coming from $d_{x^2-y^2}$ orbitals.

Because of the finite thickness of the slab, at the $\bar{M}$ point, each twin pair is represented by two doubly degenerate slab levels E_{2n-1} and E_{2n} separated by $\Delta_n = E_{2n} - E_{2n-1}$ of a few meV due to the bonding-antibonding interaction. The two pairs have different parity, so we transfer to the new basis $\Phi_{n\mu}^{\pm} = \frac{1}{\sqrt{2}}(\Psi_{2n-1\mu} \pm \Psi_{2n\mu})$, in which the original 12×12 Hamiltonian $H_{\mathbf{kp}}$ reads

$$H_{\mathbf{kp}} \longrightarrow H'_{\mathbf{kp}} = \begin{pmatrix} H_{\mathbf{kp}}^{\mathrm{Surf}(+)} & H_{\mathrm{int}} \\ H_{\mathrm{int}}^{\dagger} & H_{\mathbf{kp}}^{\mathrm{Surf}(-)} \end{pmatrix}. \tag{1}$$

The new basis functions are not parity eigenfunctions anymore, and now they are localized at one of the two surfaces of the slab denoted "+" or "−," see Fig. 1(a). By neglecting the small coupling of the surfaces due to the overlap between the + and − new basis functions, $H_{\mathrm{int}} \to 0$, we arrive at the 6×6 Hamiltonian $H_{\mathbf{kp}}^{\mathrm{Surf}(+/-)}$ for the surface states at one of the surfaces. In the following we will consider only the + surface, so we omit the superscript +. Thus, we start with the Hamiltonian for a centrosymmetric system that comprises two inversely stacked copies of a noncentrosymmetric subsystem and arrive at the reduced Hamiltonian that we ascribe to a single surface.

Note that at the $\bar{M}$ point the electron group velocities vanish by symmetry $\nabla_{\mathbf{k}} E_n = 0$, so with the proper choice of the spinor-wave-function phases [20] the above scheme can imitate a Rashba-like $\mathbf{k}\cdot\mathbf{p}$ Hamiltonian $H_{\mathbf{kp}}^{R}$ of a noncentrosymmetric system. Usually the Rashba Hamiltonian is given in a scalar basis with zero velocities at the TRIM to yield an approximate solution to the Dirac equation up to the second order in c^{-1}, see Refs. [18,19]. The SOI is considered as a perturbation, and the eigenvalues $E(\mathbf{k})$ of $H_{\mathbf{kp}}^{R}$ acquire SOI-induced nonzero slopes due to the nondiagonal terms [26]. The simplest example is the 2×2 Rashba Hamiltonian, which is readily reproduced with our method if we consider one of the three spin-orbit split surface states separately [see the 2×2 panels in Figs. 2(a) and 2(c)]:

$$H_n = \begin{pmatrix} M_n k^2 & i\alpha_n k_- \\ -i\alpha_n k_+ & M_n k^2 \end{pmatrix}, \tag{2}$$

where $k_{\pm} = k_x \pm i k_y$, and $k = \sqrt{k_x^2 + k_y^2}$. However, in our method the Rashba parameter α_n is mainly determined by the contribution coming from the matrix elements of the nonrelativistic (classical) velocity in the basis of the relativistic wave functions [27]. Still, this parameter is a measure of the Rashba effect: for $YbIr_2Si_2$ its absolute values are more than three times larger than for $YbRh_2Si_2$, as one would expect from Ir being heavier than Rh, see Table I.

The *microscopically* derived $\mathbf{k}\cdot\mathbf{p}$ Hamiltonian that covers all the considered surface states has the form

$$H_{\mathbf{kp}}^{\mathrm{Surf}} = \begin{pmatrix} E_1 + H_1 & \widetilde{H}_1 & H_0 \\ \widetilde{H}_1^{\dagger} & E_2 + H_2^{*} & \widetilde{H}_2^{\dagger} \\ H_0 & \widetilde{H}_2 & E_3 + H_3 \end{pmatrix}, \tag{3}$$

where $E_n = \epsilon_n \mathbb{I}_{2\times 2}$ and

$$\widetilde{H}_n = \begin{pmatrix} -i\tilde{\alpha}_n k_+ & d_n(\mathbf{k}) \\ -d_n^{*}(\mathbf{k}) & -i\tilde{\alpha}_n k_- \end{pmatrix}, \tag{4}$$

with $d_n(\mathbf{k}) = D_n k_+^2 - N_n k_-^2$. For the considered materials, the parameters in Eq. (3) are listed in Table I (note the opposite sign of α_3 and $\alpha_{1,2}$). The six-dimensional vectors $\mathbf{C}_{\mathbf{k}}^{\lambda}$ that

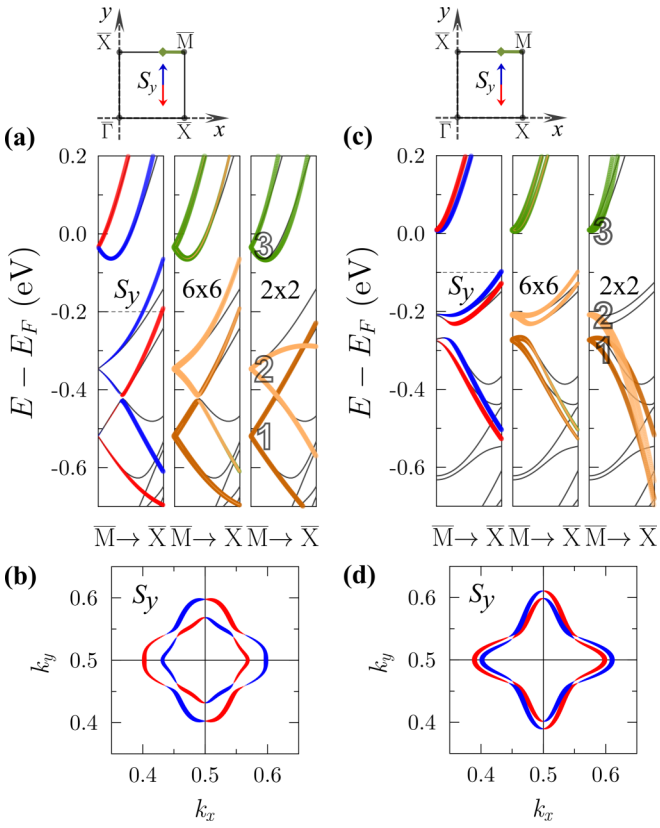

FIG. 2. Band structure of the Si-terminated surface of $YbIr_2Si_2$ (a) and $YbRh_2Si_2$ (c) by the $\mathbf{k}\cdot\mathbf{p}$ Hamiltonian (3) shown by fat bands for the momentum $\mathbf{k}$ within one-fifth of the $\bar{M}$-$\bar{X}$ interval. The CECs at -0.2 eV for $YbIr_2Si_2$ is shown in (b) and at -0.1 eV for $YbRh_2Si_2$ in (d). Blue (red) fat bands show $S_y > 0$ ($S_y < 0$) surface states $\widetilde{\Phi}^{\lambda}_{\mathbf{k}}$ of the model. The contributions form the basis states $\Phi^{+}_{n\uparrow(\downarrow)}$ with $n = 1$, 2, and 3 are shown by brown, orange, and green fat bands, respectively. Due to the symmetry, the S_x CECs are the S_y ones rotated clockwise by $\pi/2$ as in Figs. 1(f) and 1(g). Gray lines are the LDA bands.

diagonalize the Hamiltonian (3)

$$H^{\mathrm{Surf}}_{\mathbf{kp}}\mathbf{C}^{\lambda}_{\mathbf{k}} = E^{\lambda}_{\mathbf{k}}\mathbf{C}^{\lambda}_{\mathbf{k}}$$

yield the spinor solution $\widetilde{\Phi}^{\lambda}_{\mathbf{k}} = \sum_{n\mu} C^{\lambda}_{\mathbf{k}n\mu}\Phi^{+}_{n\mu}$. The calculated eigenvalues $E^{\lambda}_{\mathbf{k}}$ are shown in the 6×6 panels of Figs. 2(a) and 2(c) with the contributions $\sum_{\mu}|C^{\lambda}_{\mathbf{k}n\mu}|^2$ presented by brown, orange, and green fat bands for $n = 1$, 2, and 3, respectively. Note that the $\mathbf{k}\cdot\mathbf{p}$ calculation highly accurately reproduces the true bands over one-tenth of the $\bar{M}$-$\bar{X}$ interval.

Apart from the band dispersion curves $E^{\lambda}_{\mathbf{k}}$, our method also reproduces the *ab initio* spin structure of the surface states under study in the vicinity of the $\bar{M}$ point, Fig. 1. The spin expectation value in a state $|\widetilde{\Phi}^{\lambda}_{\mathbf{k}}\rangle$ within our Hilbert space is

$$\langle\mathbf{S}_{\mathbf{k}\lambda}\rangle = \frac{1}{2}\langle\widetilde{\Phi}^{\lambda}_{\mathbf{k}}|\boldsymbol{\sigma}|\widetilde{\Phi}^{\lambda}_{\mathbf{k}}\rangle = \frac{1}{2}\sum_{n\mu lv} C^{\lambda *}_{\mathbf{k}n\mu}C^{\lambda}_{\mathbf{k}lv}\left[\mathbf{S}^{\mathrm{Surf}}_{\mathbf{kp}}\right]^{n\mu}_{lv}, \quad (5)$$

TABLE I. Parameters of the six-band $\mathbf{k}\cdot\mathbf{p}$ Hamiltonian (based on calculations for 31-layer slabs with the lattice parameter $a = 7.583$ a.u. for $YbRh_2Si_2$ and $a = 7.624$ a.u. for $YbIr_2Si_2$). We use Rydberg atomic units: $\hbar = 2m_0 = e^2/2 = 1$.

	$YbIr_2Si_2$	$YbRh_2Si_2$
ϵ_1	−0.038	−0.020
ϵ_2	−0.026	−0.016
ϵ_3	−0.003	0.001
α_1	−0.228	−0.073
α_2	−0.126	−0.030
α_3	0.260	0.082
$\tilde{\alpha}_1$	−0.087	−0.033
$\tilde{\alpha}_2$	0.315	0.336
α_0	0.280	0.329
M_1	3.20	1.92
M_2	2.81	1.82
M_3	0.50	0.68
D_1/N_1	1.66/1.37	1.37/0.87
D_2/N_2	0.56/0.41	0.21/0.16
M_0	0.72	0.14
g^z_1/s^z_1	0.39/−0.73	0.67/−0.97
$g^{\shortparallel}_1/s^{\shortparallel}_1$	−0.62/−0.13	−0.34/−0.02
g^z_2/s^z_2	0.97/0.94	0.94/0.99
$g^{\shortparallel}_2/s^{\shortparallel}_2$	−0.19/0.02	−0.16/0.00
g^z_3/s^z_3	0.54/0.74	0.42/0.97
$g^{\shortparallel}_3/s^{\shortparallel}_3$	0.55/−0.86	0.36/−0.98
$\tilde{g}^{\shortparallel}_1/\tilde{s}^{\shortparallel}_1$	−0.69/−0.88	−0.29/−0.98
$\tilde{g}^{\shortparallel}_2/\tilde{s}^{\shortparallel}_2$	0.57/−0.35	0.97/−0.12
g^z_0/s^z_0	−0.79/−0.65	−0.09/−0.24
$g^{\shortparallel}_0/s^{\shortparallel}_0$	0.57/0.33	1.11/0.12

where $\left[\mathbf{S}^{\mathrm{Surf}}_{\mathbf{kp}}\right]^{n\mu}_{lv} = \langle\Phi^{+}_{n\mu}|\boldsymbol{\sigma}|\Phi^{+}_{lv}\rangle$ are the elements of the spin matrix [28]

$$\mathbf{S}^{\mathrm{Surf}}_{\mathbf{kp}} = \begin{pmatrix} \mathbf{S}_1 & \widetilde{\mathbf{S}}_1 & \mathbf{S}_0 \\ \widetilde{\mathbf{S}}^{*}_1 & \mathbf{S}^{*}_2 & \widetilde{\mathbf{S}}^{*}_2 \\ \mathbf{S}_0 & \widetilde{\mathbf{S}}_2 & \mathbf{S}_3 \end{pmatrix}, \quad (6)$$

with $\mathbf{S}_n = (s^{\shortparallel}_n\boldsymbol{\sigma}_{\shortparallel}, s^z_n\sigma_z)$, $\widetilde{\mathbf{S}}_n = \tilde{s}^{\shortparallel}_n\exp(i\pi\sigma_y/2)\boldsymbol{\sigma}_{\shortparallel}$, and $\boldsymbol{\sigma}_{\shortparallel} = (\sigma_x, \sigma_y)$, where σ_x, σ_y, and σ_z are the Pauli matrices. As seen in Figs. 2(a) and 2(c), with the parameters listed in Table I, the model spin structure (the blue and red fat bands) reproduces in detail the nontrivial spin polarization of the *ab initio* relativistic states, including the constant energy contours [Figs. 2(b) and 2(d)] for the transition-metal surface states, which are very different from the typical CECs of Rashba-split states. In contrast, the Si surface state has the well-known Rashba spin structure [as in Fig. 1(e)] with spin polarization less than 100% (see $s^{\shortparallel}_3$ in Table I) [29].

It is worth noting that to analyze the effect of an external magnetic field $\mathbf{B}$ the spin matrix (6) should be used in the (trivial) Zeeman term $H^{\mathrm{Surf}}_{\mathbf{kp},Z_0} = \frac{1}{2}\mu_B g_0\mathbf{S}^{\mathrm{Surf}}_{\mathbf{kp}}\cdot\mathbf{B}$, where μ_B is the Bohr magneton and $g_0 = 2.0023$ is the free-electron Landé g

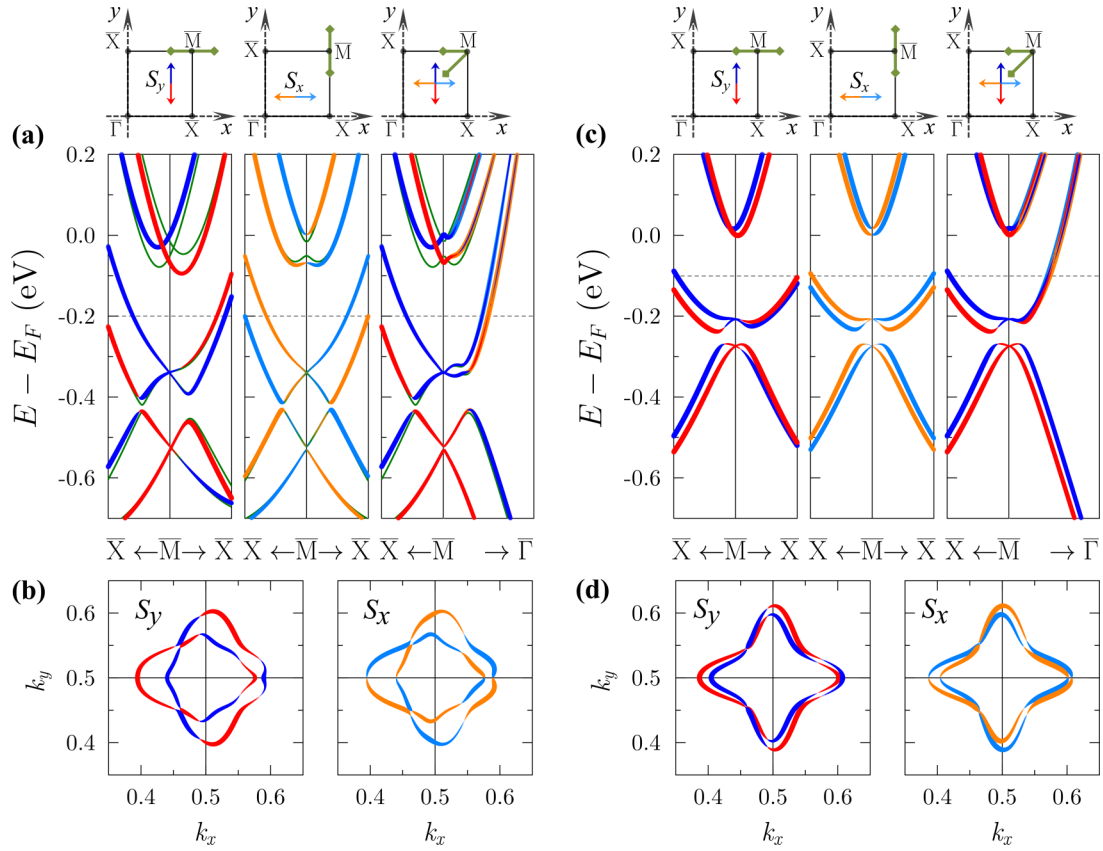

FIG. 3. Model Si-terminated surface band structure of magnetic phases of RT_2Si_2 compounds with T = Ir (a) and T = Rh (c). The $4f$ moments of the subsurface rare-earth (R) atomic layer are ferromagnetically ordered along the y axis. The effect of exchange (magnetic) interaction on the bands along $\bar{M} \to \bar{X}$ and corresponding CECs at -0.2 eV (b) and at -0.1 eV (d) is modeled by the inclusion of the trivial Zeeman term $H^{\rm Surf}_{\mathbf{kp},Z_0}$ with $\mathcal{J} = 40$ meV for T = Ir and $\mathcal{J} = 8$ meV for T = Rh. Green solid lines in (a) are the $\mathbf{k}\cdot\mathbf{p}$ bands obtained with the "indirect" exchange for electrons in the Si surface state (see text).

factor. The effective-mass contribution to the g factor [30,31] leads to the following form of the Zeeman Hamiltonian:

$$H^{\rm Surf}_{\mathbf{kp},Z} = \begin{pmatrix} H_{Z1} & \widetilde{H}_{Z1} & H_{Z0} \\ \widetilde{H}^{\dagger}_{Z1} & H^{*}_{Z2} & \widetilde{H}^{\dagger}_{Z2} \\ H_{Z0} & \widetilde{H}_{Z2} & H_{Z3} \end{pmatrix}, \tag{7}$$

where

$$H_{Zn} = \frac{\mu_B}{2}\begin{pmatrix} g^z_n B_z & g^{\shortparallel}_n B_- \\ g^{\shortparallel}_n B_+ & -g^z_n B_z \end{pmatrix}, \tag{8}$$

$$\widetilde{H}_{Zn} = \frac{\mu_B}{2}\begin{pmatrix} \tilde{g}^{\shortparallel}_n B_+ & 0 \\ 0 & -\tilde{g}^{\shortparallel}_n B_- \end{pmatrix}, \tag{9}$$

with $B_\pm = B_x \pm i B_y$. Similar to the trivial Zeeman term $H^{\rm Surf}_{\mathbf{kp},Z_0}$, this Hamiltonian can be presented as the scalar product of the magnetic field $\mathbf{B}$ and the effective g-factor matrix $\mathbf{G}^{\rm Surf}_{\mathbf{kp}}$, which has the same structure as the spin matrix (6) but with g^β_n ($\tilde{g}^\beta_n$) in place of s^β_n ($\tilde{s}^\beta_n$). The full Zeeman term $H^{\rm Surf}_{\mathbf{kp},Z_0} + H^{\rm Surf}_{\mathbf{kp},Z}$ is, thus, defined by the Hamiltonian (7) with the effective Landé g factor g^β_n ($\tilde{g}^\beta_n$) $\to g^\beta_n + g_0 s^\beta_n$ ($\tilde{g}^\beta_n + g_0\tilde{s}^\beta_n$) or, equivalently, by the term $\frac{1}{2}\mu_B(\mathbf{G}^{\rm Surf}_{\mathbf{kp}} + g_0\mathbf{S}^{\rm Surf}_{\mathbf{kp}})\cdot\mathbf{B}$. As seen in Table I, in the chosen six-band representation the effective-mass contribution to the g factor is substantially smaller than the free-electron g factor. However, for the transition-metal surface states, for the in-plane orientation of $\mathbf{B}$ this contribution can significantly enhance the effect of the external magnetic field (compared with the trivial Zeeman term), see, for example, $g^{\shortparallel}_{1(2)}$ and $s^{\shortparallel}_{1(2)}$ in Table I.

In magnetic phases of the RT_2Si_2 compounds, the four outermost atomic layers of the Si-terminated surfaces contain one rare-earth atomic layer (Eu, Gd, or Ho) with ferromagnetically ordered $4f$ moments [11,12]. This leads to the exchange interaction of surface-state electrons with magnetic moments of this monolayer. To model the magnetic exchange interaction in the presence of the Rashba effect, we treat $\boldsymbol{\mathcal{J}} = \mu_B\mathbf{B}$ as a tunable exchange interaction parameter (as, e.g., in Refs. [32,33]) in the trivial Zeeman term $H^{\rm Surf}_{\mathbf{kp},Z_0}$. An in-plane orientation of the ferromagnetically ordered $4f$ moments in the rare-earth layer is implied (specifically, along the y axis, i.e., $\boldsymbol{\mathcal{J}} = \mathcal{J}\hat{\mathbf{y}}$). By restricting the Hilbert space to the TM-surface states, for sufficiently small $\mathcal{J}$, the energy distance between the doubly degenerate states $n = 1$ and $n = 2$ at $\bar{M}$ depends on $\mathcal{J}$ as $\widetilde{\Delta} = \sqrt{(\epsilon_2 - \epsilon_1)^2 + (\mathcal{J} g_0 \tilde{s}^{\shortparallel}_1)^2}$ [34]. Each of these degenerate states acquires a splitting proportional to $\sim g_0|s^{\shortparallel}_{1(2)}\mathcal{J}|$.

We start with the Ir surface states of an RIr_2Si_2 compound and choose the value of the exchange parameter $\mathcal{J} = 40$ meV. As illustrated in Fig. 3(a), in the spectrum along the k_x axis (perpendicular to the in-plane alignment of the $4f$

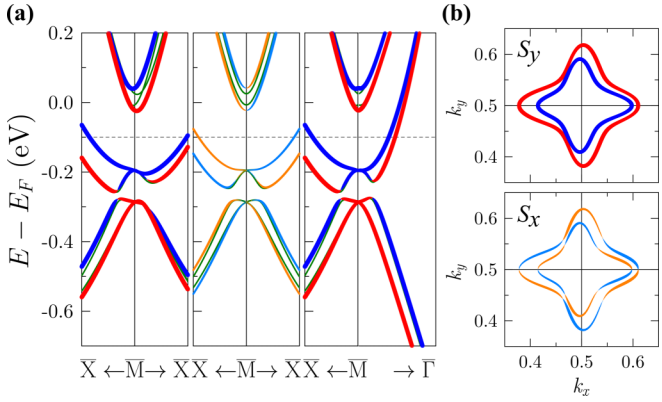

FIG. 4. Same as in Figs. 3(c) and 3(d), but for the exchange-interaction parameter $\mathcal{J} = 33$ meV and with green lines showing the effect of the "indirect" exchange for the Si surface state (see text).

moments), this is sufficient to cause a tangible asymmetry with respect to the $\bar{M}$ point. Note that the Ir surface states have a negligible splitting at the $\bar{M}$ point as a consequence of the rather small $s^{\shortparallel}_{1(2)}$ (in contrast to the Si surface state, which manifests the behavior typical of Rashba-split states in an exchange field [35]). Along the k_y axis, i.e., parallel to the magnetization direction of the ferromagnetically ordered $4f$ moments, the TM surface-state bands change slightly, retaining the symmetry with respect to $\bar{M}$ and the characteristic exotic region related to the S_x spin component. The CECs at -0.2 eV are considerably distorted, see Fig. 3(b), but the spin structure with the specific spin-momentum locking appears to be preserved.

In an $R\mathrm{Rh_2Si_2}$ compound, for the Rh surface states, a similar effect can be obtained at a substantially smaller value of $\mathcal{J} = 8$ meV, since initially they are much less separated in energy, Figs. 3(c) and 3(d). To increase the gap $\widetilde{\Delta}$ by ∼40% by switching on the exchange interaction, as is the case in the experiment on $\mathrm{EuRh_2Si_2}$ for an in-plane orientation of the $4f$ moments [12], the exchange parameter must be increased to $\mathcal{J} = 33$ meV. The resulting band dispersions and CECs are shown in Fig. 4. Note that our model gives a negligible splitting of the Rh states (∼1 meV, which cannot be experimentally resolved) in accord with the observations of Ref. [12]. Most important here is that the sign of S_y does not vary along the outer or inner CEC, and the absolute value of the spin y projection is nearly constant, Fig. 4(b). Only the specific motif of the rather small S_x component along the CECs is a remainder of the original spin-momentum locking.

III. DISCUSSION AND CONCLUSIONS

According to our model, the modification of the CECs of the TM-surface states by the magnetic exchange interaction mostly consists in stretching out along the line perpendicular to the in-plane alignment of the $4f$ moments—in opposite directions for the outer and inner CEC. With increasing the exchange parameter $\mathcal{J}$ the contours deform until they touch. A further increase of $\mathcal{J}$ lifts the degeneracy at the points of touch, and the CECs may become close in shape to those for small $\mathcal{J}$. However, for large $\mathcal{J}$ the spin is almost parallel (or antiparallel) to the magnetization direction of the ferromagnetically ordered $4f$ moments. Here the exchange interaction dominates over SOI. The stronger the SOI due to the transition-metal atoms the larger the $4f$ magnetic moment necessary to "decouple" spin from momentum. Note that in the above cases the surface states are entirely in-plane polarized, and S_z component vanishes. It becomes finite when the $4f$ magnetic moments have an out-of plane component (not shown). For example, for $R\mathrm{Rh_2Si_2}$ we found that for z orientation of the moments the parameter $\mathcal{J} = 33$ meV (close to the case of $\mathrm{HoRh_2Si_2}$ [12]) causes up to ∼90% of the out-of-plane polarization, but S_x and S_y remain substantial, with the in-plane spin-momentum locking inherent to the paramagnetic phase (the CECs also remain symmetric). For comparison, for z orientation of the moments in $R\mathrm{Ir_2Si_2}$ (as, e.g., in $\mathrm{HoIr_2Si_2}$ [36]), with $\mathcal{J} = 40$ meV, the surface states acquire up to ∼40% of the out-of-plane polarization, and their in-plane spin structure is only slightly affected.

Regarding the behavior of the transition-metal surface states, our $\mathbf{k}\cdot\mathbf{p}$ results are in full accord with the ARPES measurements on $RT_2\mathrm{Si_2}$ (with $R =$ Gd, Ho, Eu and $T =$ Rh, Ir) magnetic compounds and corresponding *ab initio* calculations [11,12,21]. Since the low-temperature magnetic phases of these compounds undergo a transition to paramagnetic phases when the temperature is increased, this was suggested to be a way to gradually tune the splitting of the states and their spin orientation in a given compound [11,12]. In our model we describe and visualize this effect by continuously changing the exchange parameter $\boldsymbol{\mathcal{J}}$ with an additional possibility to rotate the moments (simulating their different orientation in different compounds) in order to predict the modification of CEC and study the interplay between exchange and spin-orbit interaction.

In order to explicitly relate the SOI induced splitting and the effect of the magnetic field, let us introduce the analog of the "Rashba magnetic field" $\boldsymbol{\mathcal{B}}_R = (k_y, -k_x, 0)$. It allows us to rewrite the $\mathbf{k}$-linear term in the Hamiltonian (3) as $H^{\mathrm{Surf}}_{\mathbf{kp}(1)} = \boldsymbol{\mathcal{S}}_\alpha \cdot \boldsymbol{\mathcal{B}}_R$, where the matrix $\boldsymbol{\mathcal{S}}_\alpha$ has only x and y components, which reproduce the structure of the respective components of the spin matrix (6) with $s^{\shortparallel}_n$ ($\tilde{s}^{\shortparallel}_n$) replaced by α_n ($\tilde{\alpha}_n$). We can thus collect all the terms related to "spin-orbital-magnetic" interactions as the sum $\boldsymbol{\mathcal{S}}_\alpha \cdot \boldsymbol{\mathcal{B}}_R + \frac{1}{2}\mu_B(\mathbf{G}^{\mathrm{Surf}}_{\mathbf{kp}} + g_0\mathbf{S}^{\mathrm{Surf}}_{\mathbf{kp}}) \cdot \mathbf{B}$. By comparing this operator with the Hamiltonian (3), we are able to express the effect of the in-plane component of the magnetic field $\mathbf{B}$ as the conversion of the matrix elements $\mp\alpha_n k_{x,y}$ and $\mp\tilde{\alpha}_n k_{x,y}$ in Eqs. (2) and (4) into $\alpha_n(k^0_{nx,y} \mp k_{x,y})$ and $\tilde{\alpha}_n(\tilde{k}^0_{nx,y} \mp k_{x,y})$, respectively, where $-$ $(+)$ should be used for k_x (k_y). The new quantities here are the shifts in $\mathbf{k}$ space:

$$k^0_{nx,y} = \frac{\mu_B}{2\alpha_n}(g^{\shortparallel}_n + g_0 s^{\shortparallel}_n)B_{y,x},$$
$$\tilde{k}^0_{nx,y} = \frac{\mu_B}{2\tilde{\alpha}_n}(\tilde{g}^{\shortparallel}_n + g_0 \tilde{s}^{\shortparallel}_n)B_{y,x}.$$

We see that these shifts occur in the direction perpendicular to the in-plane orientation of $\mathbf{B}$, as in a classical Rashba system.

Now we turn back to our modeling of the $RT_2\mathrm{Si_2}$ magnetic compounds with the in-plane orientation of the ferromagnetically ordered $4f$ moments $\boldsymbol{\mathcal{J}} = \mathcal{J}\hat{\mathbf{y}}$. In this case we have nonzero shifts $k^0_{nx} = \mathcal{J}s^{\shortparallel}_n/\alpha_n$ and $\tilde{k}^0_{nx} = \mathcal{J}\tilde{s}^{\shortparallel}_n/\tilde{\alpha}_n$ (here $g_0/2$ is

put to unity for simplicity). This means that in the presence of the Rashba effect the sensitivity of the band dispersions to the magnetic exchange interaction $\mathcal{J}$ is stronger the larger the ratios $s_n^{\shortparallel}/\alpha_n$ and $\tilde{s}_n^{\shortparallel}/\tilde{\alpha}_n$, see Table I. For example, the sensitivities $s_n^{\shortparallel}/\alpha_n$ for $n = 1, 2$ associated with the Ir and Rh surface states are very small, less than 0.1 $\mathrm{eV}^{-1}\,\mathrm{Å}^{-1}$ (absolute value), which is related to a spin cancellation in the exotic region. Furthermore, the sensitivity of their hybridization with the Si surface state, expressed by $s_0^{\shortparallel}/\alpha_0$ and $\tilde{s}_2^{\shortparallel}/\tilde{\alpha}_2$, is also rather small, around 0.2 $\mathrm{eV}^{-1}\,\mathrm{Å}^{-1}$. At the same time, for the Si surface state the absolute value of the ratio $s_3^{\shortparallel}/\alpha_3$ is 0.5 $\mathrm{eV}^{-1}\,\mathrm{Å}^{-1}$ for $R\mathrm{Ir}_2\mathrm{Si}_2$ and even 1.7 $\mathrm{eV}^{-1}\,\mathrm{Å}^{-1}$ for $R\mathrm{Rh}_2\mathrm{Si}_2$. As a result, see Figs. 3(a) and 3(c), the degeneracy point of the Si surface state shifts by $k_{3x}^0 = -0.02$ $\mathrm{Å}^{-1}$ and -0.01 $\mathrm{Å}^{-1}$, respectively, away from $\bar{M}$, while those of the TM-related surface states stay almost unaffected. However, in each compound, the strongest sensitivity is observed for the hybridization between the TM-related surface states $\tilde{s}_1^{\shortparallel}/\tilde{\alpha}_1 =$ 1.4 (4.1) $\mathrm{eV}^{-1}\,\mathrm{Å}^{-1}$ for the Ir (Rh) surface states. It is the high sensitivity of these states that is responsible for their modifications by the magnetic exchange interaction.

Our model can be further refined by considering the density profiles of the surface states. For example, as seen in Fig. 1(a), there is a negligible direct overlap of the Si surface state with the rare-earth layer. Therefore, the exchange interaction that couples the electrons in this state with $4f$ moments may act through an intermediary, whose role can be played by subsurface transition-metal electrons. For such indirect exchange, the parameter $\mathcal{J}$ may differ (in value and even in sign) from that for the TM states. Indeed, for the Si surface state, a two times smaller exchange interaction $\mathcal{J}$ of the opposite sign makes the spectra much more consistent with *ab initio* calculations for $R\mathrm{Rh}_2\mathrm{Si}_2$ magnetic compounds with $R =$ Eu, Gd, Ho [11,12], see green lines in Figs. 3(a) and 4(a).

It is noteworthy that in the transition-metal plane the true unit cell, which we use in our *ab initio* calculations, contains two TM sublattices, Fig. 5(a). The corresponding surface Brillouin zone (SBZ) can be thought of as a folded SBZ (as, e.g., in Ref. [37]), so one can imagine an effective unit cell with one TM atom and a bigger unfolded SBZ (USBZ), see Fig. 5(b). In this case, the $\bar{M}$ point of the SBZ corresponds to the $\bar{X}$ point of the USBZ ($\bar{X}'$), while the $\bar{M}$ point of the USBZ ($\bar{M}'$) coincides with the $\bar{\Gamma}$ point, since the $\bar{X}$-$\bar{M}'$ line folds into the $\bar{\Gamma}$-$\bar{X}$ one. The $\bar{X}'$-$\bar{M}'$ line is superimposed on $\bar{\Gamma}$-$\bar{M}$. The $\bar{Y}$ direction (the $\bar{X}$-$\bar{M}$ line) is, thus, the fold of the "envelope," Fig. 5(b).

We now decompose the momentum-dependent spin expectation value of the $n = 1$ and $n = 2$ states into contributions from each of the two sublattices and show them with spin-resolved fat bands in Fig. 5(c). Along the $\bar{M}$-$\bar{X}$ line, in the exotic region around the $\bar{M}$ point, we see the typical Rashba *spin* splitting. Within our effective model, the presented sublattice-resolved spin structure can be perfectly reproduced (not shown) by manually setting the parameters of the spin matrix (6) for these states as $s_1^{\shortparallel} = -s_2^{\shortparallel} = s_R^{\shortparallel}$, where $s_R^{\shortparallel} = |s_3^{\shortparallel}|$ for sublattice A and $s_R^{\shortparallel} = -|s_3^{\shortparallel}|$ for sublattice B, i.e., is a typical Rashba in-plane spin polarization. One may now look at the TM surface states from the point of view of the classical Rashba Hamiltonian and use the spin expectation value at one of the TM sublattices as a dynamic variable. Such a model, however, would suffer from an ambiguity because the Rashba parameter has a different sign depending on what sublattice one chooses to define spin. This means that in the $RT_2\mathrm{Si}_2$ compounds (with $T=$ Ir or Rh) the resulting (total) spin structure of the TM-surface states in close vicinity of $\bar{M}$ has a vanishing in-plane spin expectation value due to an almost total cancellation of the contributions from the sublattices with the opposite spin polarization. This can be considered as a vivid example of a phenomenon known as a hidden spin polarization [38], which here is associated with two symmetry related sublattices of a single layer.

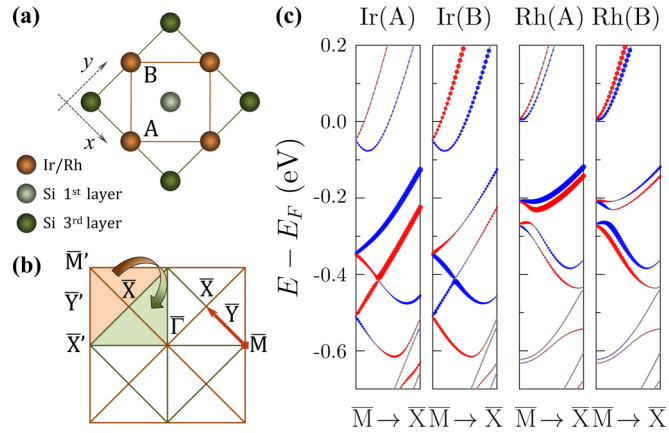

FIG. 5. (a) Projection of the outermost three layers of the Si-terminated surface onto the transition-metal atomic plane. (b) True (folded, green) and effective (unfolded, brown) Brillouin zones corresponding to the 2D unit cells highlighted green and brown in (a), respectively. Red arrow marks the treated $\bar{M}$-$\bar{X}$ direction. (c) Spin-resolved contribution from the sublattices "A" and "B" of the transition-metal subsurface layer as obtained from LDA calculations for $\mathrm{YbIr}_2\mathrm{Si}_2$ and $\mathrm{YbRh}_2\mathrm{Si}_2$. Blue (red) fat bands correspond to $S_y > 0$ ($S_y < 0$) 31-layer slab states.

To summarize, we have developed an effective model for the Si-terminated surface states of the rare-earth ternary compounds based on the fully *ab initio* $\mathbf{k}\cdot\mathbf{p}$ perturbation approach to generate model Hamiltonians of a desired size. We have extended the approach to make the model capable of correctly reproducing the true spin polarization of the spin-orbit split states under study. This improvement also enables a proper treatment of the effect of exchange interaction of surface-state electrons with a ferromagnetic monolayer. By applying our model to the surface states of the $RT_2\mathrm{Si}_2$ compounds with $T=$ Ir or Rh, we have demonstrated how their relativistic splitting and spin polarization not typical of the Rashba effect depend on the relative strength of the competing spin-orbit and exchange interactions.

ACKNOWLEDGMENTS

The authors are grateful to S. Schulz, M. Güttler, and D. Vyalikh for the useful discussions and critical reading of this manuscript. This work was supported by the Spanish Ministry of Science, Innovation and Universities (Project No. FIS2016-76617-P).

[1] A. Manchon, H. C. Koo, J. Nitta, S. M. Frolov, and R. A. Duine, New perspectives for Rashba spin-orbit coupling, Nat. Mater. **14**, 871 (2015).

[2] E. E. Krasovskii, Spin-orbit coupling at surfaces and 2D materials, J. Phys.: Condens. Matter **27**, 493001 (2015).

[3] A. Soumyanarayanan, N. Reyren, A. Fert, and C. Panagopoulos, Emergent phenomena induced by spin-orbit coupling at surfaces and interfaces, Nature (London) **539**, 509 (2016).

[4] F. Ortmann, S. Roche, and S. O. Valenzuela, *Topological Insulators, Fundamentals and Perspectives* (Wiley, New York, 2015).

[5] S. V. Eremeev, S. S. Tsirkin, I. A. Nechaev, P. M. Echenique, and E. V. Chulkov, New generation of two-dimensional spintronic systems realized by coupling of Rashba and Dirac fermions, Sci. Rep. **5**, 12819 (2015).

[6] Y. Ren, Z. Qiao, and Q. Niu, Topological phases in two-dimensional materials: A review, Rep. Prog. Phys. **79**, 066501 (2016).

[7] A. Bansil, H. Lin, and T. Das, Colloquium: Topological band theory, Rev. Mod. Phys. **88**, 021004 (2016).

[8] I. A. Nechaev, S. V. Eremeev, E. E. Krasovskii, P. M. Echenique, and E. V. Chulkov, Quantum spin Hall insulators in centrosymmetric thin films composed from topologically trivial BiTeI trilayers, Sci. Rep. **7**, 43666 (2017).

[9] I. A. Nechaev and E. E. Krasovskii, Spin filtering via resonant reflection of relativistic surface states, Phys. Rev. B **97**, 041407 (2018).

[10] S. Danzenbächer, D. V. Vyalikh, K. Kummer, C. Krellner, M. Holder, M. Höppner, Yu. Kucherenko, C. Geibel, M. Shi, L. Patthey, S. L. Molodtsov, and C. Laubschat, Insight into the f-Derived Fermi Surface of the Heavy-Fermion Compound $YbRh_2Si_2$, Phys. Rev. Lett. **107**, 267601 (2011).

[11] M. Güttler, A. Generalov, M. M. Otrokov, K. Kummer, K. Kliemt, A. Fedorov, A. Chikina, S. Danzenbächer, S. Schulz, E. V. Chulkov, Yu. M. Koroteev, N. Caroca-Canales, M. Shi, M. Radovic, C. Geibel, C. Laubschat, P. Dudin, T. K. Kim, M. Hoesch, C. Krellner, and D. V. Vyalikh, Robust and tunable itinerant ferromagnetism at the silicon surface of the antiferromagnet $GdRh_2Si_2$, Sci. Rep. **6**, 24254 (2016).

[12] A. Generalov, M. M. Otrokov, A. Chikina, K. Kliemt, K. Kummer, M. Höppner, M. Güttler, S. Seiro, A. Fedorov, S. Schulz, S. Danzenbächer, E. V. Chulkov, C. Geibel, C. Laubschat, P. Dudin, M. Hoesch, T. Kim, M. Radovic, M. Shi, N. C. Plumb, C. Krellner, and D. V. Vyalikh, Spin orientation of two-dimensional electrons driven by temperature-tunable competition of spin-orbit and exchange-magnetic interactions, Nano Lett. **17**, 811 (2017).

[13] A. Chikina, A. Generalov, K. Kummer, M. Güttler, V. N. Antonov, Yu. Kucherenko, K. Kliemt, C. Krellner, S. Danzenbächer, T. Kim, P. Dudin, C. Geibel, C. Laubschat, and D. V. Vyalikh, Valence instability in the bulk and at the surface of the antiferromagnet $SmRh_2Si_2$, Phys. Rev. B **95**, 155127 (2017).

[14] A. Generalov, J. Falke, I. A. Nechaev, M. M. Otrokov, M. Güttler, A. Chikina, K. Kliemt, S. Seiro, K. Kummer, S. Danzenbächer, D. Usachov, T. K. Kim, P. Dudin, E. V. Chulkov, C. Laubschat, C. Geibel, C. Krellner, and D. V. Vyalikh, Strong spin-orbit coupling in the noncentrosymmetric Kondo lattice, Phys. Rev. B **98**, 115157 (2018).

[15] I. Felner and I. Nowik, Itinerant and local magnetism, superconductivity and mixed valency phenomena in RM_2Si_2 (R = rare earth, M = Rh, Ru), J. Phys. Chem. Solids **45**, 419 (1984).

[16] O. Trovarelli, C. Geibel, S. Mederle, C. Langhammer, F. M. Grosche, P. Gegenwart, M. Lang, G. Sparn, and F. Steglich, $YbRh_2Si_2$: Pronounced Non-Fermi-Liquid Effects above a Low-Lying Magnetic Phase Transition, Phys. Rev. Lett. **85**, 626 (2000).

[17] Z. Hossain, O. Trovarelli, C. Geibel, and F. Steglich, Complex magnetic order in $EuRh_2Si_2$, J. Alloys Compd. **323-324**, 396 (2001), Proceedings of the 4th International Conference on f-Elements.

[18] E. I. Rashba and V. I. Sheka, Symmetry of energy bands in crystals of wurtzite type II. Symmetry of bands with spin-orbit interaction included, Fiz. Tverd. Tela: Collected Papers **2**, 62 (1959).

[19] Yu. A. Bychkov and E. I. Rashba, Properties of a 2D electron gas with lifted spectral degeneracy, JETP Lett. **39**, 78 (1984).

[20] I. A. Nechaev and E. E. Krasovskii, Relativistic $\mathbf{k}\cdot\mathbf{p}$ Hamiltonians for centrosymmetric topological insulators from *ab initio* wave functions, Phys. Rev. B **94**, 201410 (2016).

[21] S. Schulz, I. A. Nechaev, M. Güttler, G. Poelchen, A. Generalov, S. Danzenbächer, A. Chikina, S. Seiro, K. Kummer, A. Yu. Vyazovskaya, T. K. Kim, P. Dudin, E. V. Chulkov, C. Laubschat, E. E. Krasovskii, C. Geibel, C. Krellner, and D. V. Vyalikh, Emerging 2D-ferromagnetism and strong spin-orbit coupling at the surface of mixed-valent $EuIr_2Si_2$, (unpublished) (2018).

[22] We believe that the calculated surface electronic spectrum of $YbRh_2Si_2$ does not strongly depend on the presence of the antiferromagnetic order below $T_N \simeq 65$ mK with a weak Yb^{3+} moment of $2\times10^{-3}\mu_B$ [16,39].

[23] C. Krellner, S. Taube, T. Westerkamp, Z. Hossain, and C. Geibel, Single-crystal growth of $YbRh_2Si_2$ and $YbIr_2Si_2$, Philos. Mag. **92**, 2508 (2012).

[24] E. E. Krasovskii, Accuracy and convergence properties of the extended linear augmented-plane-wave method, Phys. Rev. B **56**, 12866 (1997).

[25] E. E. Krasovskii, F. Starrost, and W. Schattke, Augmented Fourier components method for constructing the crystal potential in self-consistent band-structure calculations, Phys. Rev. B **59**, 10504 (1999).

[26] For noncentrosymmetric systems, relativistic spinor wave functions taken as unperturbed eigenfunctions give the major contribution to the slope already at the nonrelativistic (classical) level [27].

[27] E. E. Krasovskii, Microscopic origin of the relativistic splitting of surface states, Phys. Rev. B **90**, 115434 (2014).

[28] Note that for a scalar(-relativistic) basis the matrix elements $[\mathbf{S}^{\rm Surf}_{\mathbf{kp}}]^{n\mu}_{l\nu} = \delta_{nl}[\boldsymbol{\sigma}]^{\mu}_{\nu}$.

[29] As follows from our calculations done in Ref. [20] for six-quintuple-layer slabs, within the 2×2 model description the surface states of the topological insulators Bi_2Se_3, Bi_2Te_3, and Sb_2Te_3 are characterized by $\mathbf{S}^{\rm Surf}_{\mathbf{kp}} = (s^{\shortparallel}\boldsymbol{\sigma}_{\shortparallel}, s^z\sigma_z)$ with $s^{\shortparallel}(s^z) = 0.70(0.40)$, 0.60(0.20), and 0.63(0.26), respectively.

[30] R. Winkler, *Spin-Orbit Coupling Effects in Two-Dimensional Electron and Hole Systems* (Springer, Berlin, 2003).

[31] L. C. Lew Yan Voon and M. Willatzen, *The k·p Method: Electronic Properties of Semiconductors* (Springer, Berlin, 2009).

[32] R. L. Hota, G. S. Tripathi, and J. N. Mohanty, Theory of effective g factors and effective masses in diluted magnetic semiconductors, Phys. Rev. B **47**, 9319 (1993).

[33] A. Manchon and S. Zhang, Theory of spin torque due to spin-orbit coupling, Phys. Rev. B **79**, 094422 (2009).

[34] With the experimental data reported in Ref. [12] for the magnetic phase of $EuRh_2Si_2$, the formula for $\widetilde{\Delta}$ gives the value of the exchange parameter of $\mathcal{J} \sim 70$ meV.

[35] O. Krupin, G. Bihlmayer, K. M. Döbrich, J. E. Prieto, K. Starke, S. Gorovikov, S. Blügel, S. Kevan, and G. Kaindl, Rashba effect at the surfaces of rare-earth metals and their monoxides, New J. Phys. **11**, 013035 (2009).

[36] K. Kliemt, M. Bolte, and C. Krellner, Magnetic anisotropy in $HoIr_2Si_2$ ($I4/mmm$), arXiv:1807.03657.

[37] H. Eschrig and K. Koepernik, Tight-binding models for the iron-based superconductors, Phys. Rev. B **80**, 104503 (2009).

[38] X. Zhang, Q. Liu, J.-W. Luo, A. J. Freeman, and A. Zunger, Hidden spin polarization in inversion-symmetric bulk crystals, Nat. Phys. **10**, 387 (2014).

[39] K. Ishida, D. E. MacLaughlin, B.-L. Young, K. Okamoto, Y. Kawasaki, Y. Kitaoka, G. J. Nieuwenhuys, R. H. Heffner, O. O. Bernal, W. Higemoto, A. Koda, R. Kadono, O. Trovarelli, C. Geibel, and F. Steglich, Low-temperature magnetic order and spin dynamics in $YbRh_2Si_2$, Phys. Rev. B **68**, 184401 (2003).